scientific reports

Check for updates

OPEN

Synthesis of a cross-linked polymer using a diallylammonium monomer containing 12-crown-4 motifs for the selective extraction of lithium ions

Khaled M. Ossoss, Mohammad N. Siddiqui & Shaikh A. Ali✉

A new diallyl amine salt monomer (I) bearing Li^+ chelating 12-Crown-4 ether motifs [$(H_2C=CHCH_2)_2NH^+CH_2$-(12-C-4) Cl^-] was synthesized. Monomer (I) under free radical cyclopolymerization and alternate copolymerization with SO_2 afforded homo (II) and copolymer (III) in good yields. Terpolymerization of I, SO_2, and a cross-linker tetraallylhexane-1,6-diammonium chloride (IV) gave cross-linked resin V, which has been utilized as a scavenger for lithium ions from aqueous samples via the liquid–solid technique. Optimizing a method involves adjusting multiple variables, such as pH, Li^+ concentration, and resin dose, to achieve the best possible results. The adsorption capacity was determined using inductively coupled plasma-optical emission spectroscopy (ICP–OES). The lithium removal study was conducted at concentrations ranging from 20 to 100 ppm. Resin V adsorbs lithium ions rapidly with excellent efficiency following second-order kinetics and fitting the Temkin and Langmuir adsorption isotherms. The resin demonstrated remarkable selectivity in adsorbing Li^+ from its binary mixtures Li^+/Na^+ and Li^+/K^+.

Keywords 12-Crown-4-ether, Lithium ion, Diallyl amine salts, Selective extraction, Cyclopolymerization

Lightweight lithium-ion batteries (LIBs) with cathode electrode material $LiCoO_2$ are extensively used in various electronic devices including electric vehicles[1,2]. LIBs are high-energy storage materials[3,4] owing to their low memory effect and long service life[5,6]. The Demand for LIBs has risen dramatically; the electric cars in China alone surpassed 2 million by 2020[7] and is predicted to exceed 300 million globally by 2030[8]. Rapid growth will eventually lead to an enormous number of spent LIBs[9] thereby causing environmental pollution and the depletion of natural resources[10]. For sustainability, spent LIBs must be recycled[11] since an average of 5 weight% is lithium[12].

Salt brine accounts for 69% of the world's lithium reserves[13]. Lithium is recovered from various primary resources via several protocols[14,15]. Recovery processes involving hydrometallurgy and pyrometallurgy have been proposed to recycle valuable materials from waste LIBs[16,17].

Exposure to lithium ions causes serious damage to human health[18] thereby requiring their removal and recycling from industrial wastewater produced by the disposal of spent LIBs. Cost-effective and environmentally friendly methods must be developed for trapping Li^+ selectively from coexisting alkali and alkaline earth metals in the Salt Lake brine. An effective process is essential for extracting low lithium concentrations from seawater and industrial and mining wastewater[19].

Crown ethers (CEs) as cyclic polyethers have a hydrophobic ring surrounding a hydrophilic cavity. The unshared electron pairs of oxygen atoms can form host–guest complexes by selectively coordinating the s-block elements[20,21]. The manufacturing of CEs and their metal ion complexing properties[22] focus on the electrostatic attraction between the cation and the oxygen lone pairs of the CEs leading to the metal complexes via the combined effects of chemical and physical sorption of the metal cations. Matching of cavity sizes of 12- to 14-membered CEs in the range of 1.2–1.5 Å and Li^+ with an ionic diameter of 1.36 Å leads to its selective complexation[23].

Chemistry Department and Interdisciplinary Research Center for Refining and Advanced Chemicals, King Fahd University of Petroleum & Minerals (KFUPM), Dhahran 31261, Saudi Arabia. ✉email: shaikh@kfupm.edu.sa

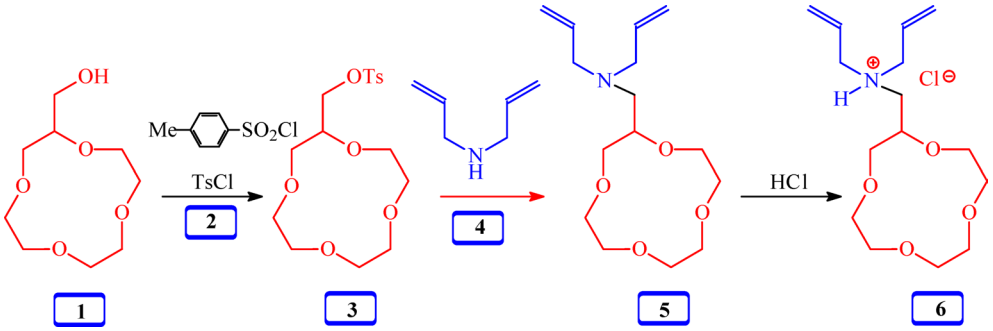

Scheme 1. Preparation of a diallyl amine salt Functionalized with a methyl 12-crown-4 ether pendant group (compound **6**).

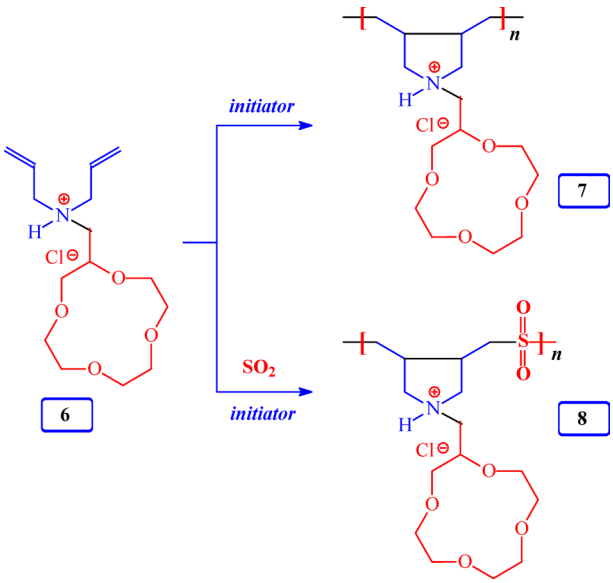

Scheme 2. Synthesis of homopolymer **7** and the copolymer with SO_2**8**.

Liquid–liquid extraction or liquid membrane systems integrated with CEs utilize toxic organic solvents[24,25]. They have low to moderate extraction efficiency. However, the solid-liquid extraction is associated with a high separation factor and can be recycled[26]. Polymers decorated with CEs as pendants have been utilized in various membrane-based separation applications[27,28] including the trapping of Li^+ from wastewater[29] and have a high adsorption capacity (4.07 mg g^{-1}). A Li^+-imprinted material demonstrated a q_m value of 16.4 mg g^{-1} from its 40 ppm Li^+ solution[30].

In this work, 12-crown-4-derived diallylammonium monomer **6** was synthesized (Scheme 1). Polymers **7** and **8** and novel resins (i.e., cross-linked) **10** and **11** (Schemes 2, 3) bearing motifs of Aliphatic 12-crown-4 have been synthesized *via* Butler's cyclopolymerization protocol[31]. Polymers incorporating five-membered cyclic structures within their main chains have been acknowledged as the eighth fundamental class of synthetic polymer architectures[32,33]. To our knowledge, the materials used in this work are the first to feature a combination of strongly coordinating ether and amine groups, along with weakly coordinating sulfone (SO_2) groups. Resin **11** was examined for its capability to adsorb lithium ions (Li^+) from aqueous solutions *via* a solid–liquid separation approach. Furthermore, lithium desorption from the cross-linked polymer (resin **11**) was investigated to explore the recovery of Li^+ ions and the potential recycling of the resin.

Experimental details

Chemicals and materials

2-(Hydroxymethyl)−12-crown-4-ether from TCI Chemicals (Tokyo Chemical Industry), p-toluene sulfonyl chloride (tosyl chloride) from Alfa Aesar, LiCl from BDH Company, HCl and NaCl from Fisher Scientific Company, 2,2′-Azobis(2-methylpropionamidine) dihydrochloride (AMPD), ammonium persulfate (APS), 2,2′-azobis(2-methylpropionitrile) (AIBN), diallylamine, KCl and $MgCl_2$ from Sigma Aldrich were purchased. Tetraallylhexane-1,6-diammonium chloride monomer was synthesized as described previously[34]. All glassware was cleaned with water (deionized).

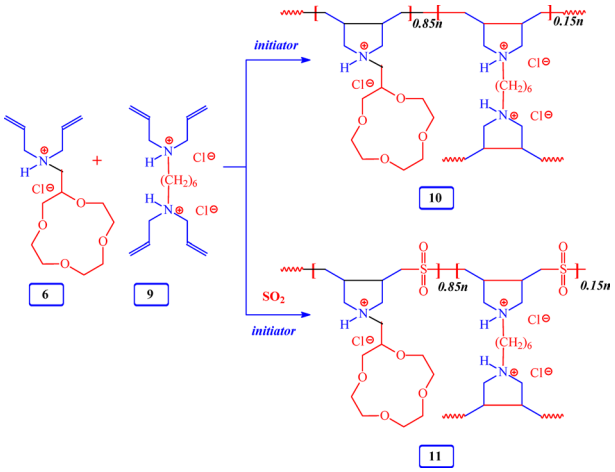

Scheme 3. Synthesis of cross-linked resin bearing residues of 12-crown-4-ether.

Physical methods

A ThermoFisher Scientific™ Nicolet™ iS10 FTIR spectrometer was utilized to obtain the IR spectra. The NMR spectra were measured with a 600-MHz JEOL spectrometer. Thermogravimetric analysis (TGA) under a N_2 flow (50 mL/min) and a temperature change of 10 °C/min in the range 20–800 °C was accomplished using an SDT analyzer (TA instruments, Model: Q600). Elemental analyses of the samples were performed in a Perkin Elmer instrument (Series II Model 2400). Viscosity measurements at 30.0 ± 0.1 °C were carried out *via* a Ubbelohde viscometer (Viscometer Constant = 0.005 cSt/s) in a water bath (CT72/P, SI Analytics, Germany). At each concentration, at least triplicate measurements were taken to maintain < 0.2% error in time. The pHs of the solutions were measured using an Oakton pH meter.

Scanning electron microscopy (SEM) images were captured on a THERMO QUATRRO S (ThermoFisher TM Scientific). For morphological characteristics, the microscope, which was equipped with an energy dispersive X-ray spectrometer (EDX, Oxford Inc.), was operated in backscattered electron mode at different accelerating voltages and working distances. Before analysis, the samples were sprinkled on double-sided adhesive tape and coated with a thin layer of gold for 10 s. ICP-OES - an Optima 8000 from Perkin Elmer - was used to determine the lithium concentrations. The specifications were as follows: light source: axial view, torch; detector: two-dimensional Echelle semiconductor detector (CCD); wavelength range: 165–800 nm; RF power: 40 MHz; 750–1500 W. An ESCALAB™ 250Xi X-ray photoelectron spectrometer (Thermo Scientific) with monochromatic micro-focused Al Kα as an X-ray source was used for XPS analysis. The C 1 s peak at 284.8 eV was taken as a reference to calibrate the XPS spectra. Organic solvents of HPLC grade and double distilled water (Millipore, 18.2 MΩ·cm) were utilized.

Synthesis of 2-(tosyloxymethyl)–12-crown-4-ether (3)

Tosyl chloride **2** (1.14 g, 6.0 mmol) and KOH (1.12 g, 20 mmol) were added to a solution of 2-(hydroxymethyl)–12-crown-4-ether **1** (1.02 g, 5.0 mmol) in CH_2Cl_2 (DCM) (40 mL) at 0 °C and stirred at 25 °C for 24 h. After washing the heterogeneous mixture with water (3 × 10 mL), the DCM layer after drying (Na_2SO_4) and concentration afforded tosylate derivative **3** (colorless oil, 1.9 g, 95%). The above reaction was repeated several times to synthesize more of compound **3**. ν_{max} (neat): 2861, 1597, 1495, 1ed450, 1356, 1189, 1175, 1131, 1096, 1073, 1019, 974, 919, 815, 788, 734 and 705 cm^{-1}; δ_H ($CDCl_3$): 2.43 (3 H, s), 3.43–3.87 (15 H, m), 3.99 (2 H, dq), 7.32 (2 H, d), 7.77 (2 H, d), ($CDCl_3$ at 7.25); δ_C ($CDCl_3$): 144.98 (1 C), 132.84 (1 C), 129.97 (1 C), 129.91 (1 C), 128.10 (2 C), 77.18 (1 C), 71.13–70.22 (7 C), 69.76 (1 C), 21.76 (1 C). ($CDCl_3$ middle C: 77.14).

Synthesis of 2-(diallylaminomethyl)–12-crown-4-ether (5)

A solution of diallyl amine **4** (14.2 g, 146 mmol) and tosylate derivative **3** (8.6 g, 23.9 mmol) in acetonitrile (AN) (35 mL) in a closed RB flask purged with N_2 was stirred at 75 °C (20 h) and 85 °C (24 h). After the removal of AN and excess diallylamine, the residue was taken up in a saturated $(NH_4)_2CO_3$ (20 mL) and extracted with DCM (3 × 30 mL). After drying (Na_2SO_4) and concentrating the combined organic layer, the residue was purified by chromatography (silica, 95:5 ether/methanol) to obtain **5** (colorless liquid, 5.7 g, 83%). [Found: C, 62.8; H, 9.7; N, 4.8%. $C_{15}H_{27}NO_4$ requires C, 63.13; H, 9.54; N, 4.91%]. ν_{max} (neat): 3075, 2906, 2856, 1642, 1447, 1418, 1357, 1302, 1253, 1125, 995, 972, 915 and 863 cm^{-1}; δ_H ($CDCl_3$): 2.34 (dd, 1 H, *J* 6.6, 13.8 Hz), 2.41 (dd, 1 H, *J* 5.7, 13.8 Hz), 3.00 (dd, 2 H, *J* 6.6, 13.8 Hz), 3.06 (dd, 2 H, J 6.0, 13.8 Hz), 3.34 (dd, 1 H, J 8.1, 11.1 Hz), 3.52–3.76 (14 H, m), 5.05 (4 H, m), 5.74 (2 H, m);δ_C ($CDCl_3$): 135.82 (2 C, *C*H = CH_2), 117.48 (2 C, CH = *C*H_2), 78.15 (1 C), 73.15 (1 C), 71.25–69.62 (6 C), 57.85 (2 C, CH_2-CH = CH_2), 54.37 (1 C), ($CDCl_3$ middle C: 77.23).

Synthesis of 2-(diallylaminomethyl)–12-crown-4-ether hydrochloride (6)

After the dropwise addition of HCl (37%, 2.06 g, 20.9 mmol) to the crown ether **5** (4.98 g, 17.4 mmol)/water (15 mL) mixture, it was stirred at 23 °C (30 min) and freeze-dried to afford monomer **6** (colorless liquid, 5.4 g,

96%). [Found: C, 55.6; H, 8.9; N, 4.2%. $C_{15}H_{28}ClNO_4$ requires C, 55.98; H, 8.77; N, 4.35%]. ν_{max} (neat): 3420, 2861, 2360, 1646, 1456, 1358, 1296, 1249, 1125, 1098, 997, 942 and 837 cm^{-1}; δ_H (D_2O): 3.93–3.03 (21 H, m), 5.44 (4 H, m), 5.76 (2 H, m), (D_2O at 4.68); δ_C (D_2O): 127.06 (1 C, CH = CH_2), 126.86 (1 C, CH = CH_2), 125.60 (1 C, CH = CH_2), 125.21 (1 C, CH = CH_2), 72.87 (1 C), 70.15–68.15 (7 C), 66.60 (dioxane), 56.90 (1 C, CH_2-CH = CH_2), 54.81 (1 C, CH_2-CH = CH_2), 53.19 (1 C).

Synthesis of homopolymer (7)

The initiator APS (100.0 mg) was added to monomer **6** (700 mg, 2.17 mmol)/H_2O (400 mg) solution in a 5 mL-RB flask at 100 °C. After a 2-min interval, more APS (75 mg) was added and stirred at 100 °C for 20 min. Upon dialysis (Spectra/Por membrane tube: MWCO 1000 Da) of the resulting crude polymer against distilled water (12 h), polymer **7** was obtained by freeze drying as a light brown hygroscopic solid (450 mg, 64%). [Found: C, 55.5; H, 9.0; N, 4.3%. $C_{15}H_{28}ClNO_4$ requires C, 55.98; H, 8.77; N, 4.35%].ν_{max} (KBr): 3387, 2924, 2717, 2081, 1639, 1457, 1364, 1300, 1254, 1133, 915, 842 and 620 cm^{-1}.

Synthesis of copolymer (8) using monomer 6 and SO_2

SO_2 (234 mg, 3.66 mmol) was absorbed onto a monomer **6** (644 mg, 2.0 mmol)/DMSO (750 mg) solution in a 10 mL-RB flask. After AIBN (15 mg) was introduced, the mixture in the closed flask was stirred (65 °C, 24 h). The resulting polymer was dialyzed in a Spectra/Por membrane tube (MWCO 1000 Da) against distilled water (6 h). Copolymer **8** was obtained by freeze drying as a light brown semisolid (503 mg, 65%). [Found: C, 46.3; H, 7.4; N, 3.5; S, 8.0%. $C_{15}H_{28}ClNO_6S$ requires C, 46.69; H, 7.31; N, 3.63; S, 8.31%].ν_{max} (KBr): 3433, 2920, 1644, 1458, 1411, 1363, 1307, 1129, 1030, 915, 859, 618 and 513 cm^{-1}.

Synthesis of cross-linked resin (10)

A solution of **6** (805 mg, 2.5 mmol) and the cross-linker tetraallylhexane-1,6-diammonium chloride monomer **9** (154 mg, 0.44 mmol) in H_2O (562 mg) in a 10 mL-RB flask was heated to 100 °C; thereafter, APS (155 mg) was added. After 2 min, an additional amount of APS (100 mg) was added, and the mixture was stirred at 100 °C (6 h) under N_2. After washing with water, resin **10** was dried in vacuo at 55 °C (light brown hygroscopic solid, 594 mg, 61%). [Found: C, 56.1; H, 9.1; N, 4.7; S, 8.0%. Monomers **9** and **6** incorporated in an 85:15 ratio require C, 56.92; H, 8.94; N, 4.94%]. ν_{max} (KBr): 3390, 2923, 2863, 2511, 1644, 1455, 1359, 1026, 837 and 606 cm^{-1}.

Synthesis of cross-linked resin (11)

After absorbing SO_2 (655 mg, 10.2 mmol) onto a solution of **6** (1.25 g, 3.88 mmol) and **9** (241 mg, 0.69 mmol) in DMSO (2.0 g, 27.4 mmol) in a 50 mL-RB flask and adding AIBN (70 mg), the mixture was heated in the closed flask at 65 °C (24 h) and 75 °C (6 h). The mixture was dialyzed in a Spectra/Por membrane tube (MWCO 1000 Da) against distilled water (12 h). The separated resin was dried in vacuo at 55 °C to obtain resin **11** (creamy white solid) (1.5 g, 80%). [Found: C, 45.7; H, 7.4; N, 3.9; S, 8.9%. Monomers 9 and 6 and SO_2 incorporated at an 85:15:115 mol ratio require C, 46.43; H, 7.29; N, 4.03; S, 9.23%]. ν_{max} (KBr): 3390, 2917, 2858, 2444, 1704, 1644, 1452, 1360, 1300, 1120, 1022, 837 and 605 cm^{-1}.

Evaluation of adsorption performance

Adsorption of Li^+ ions

Several concentrations at the ppm level were prepared from a 100 ppm Li^+ ion stock solution (LiCl). The adsorption capacities (q_e) in mg g^{-1} were determined *via* Eq. (1), where C_o and C_e in mg L^{-1} represent the initial and equilibrium concentrations of Li^+ ions, respectively; the solution volume is V in L; and m is the mass of the resin (g).

$$q_e = (C_o - C_e) \times \frac{V}{m} \tag{1}$$

The extraction efficiency (E%) was determined *via* Eq. (2).

$$E\% = \frac{(C_o - C_e)}{C_o} \times 100 \tag{2}$$

Adsorption experiments involved resin **11** (50 mg) and 20 ppm Li^+ solution (10 mL) contained in screw-capped glass vials. The mixtures were continuously stirred at 200 rpm (1 h, 23 °C). The pH was adjusted to 7.0 using either 0.01 N NH_4OH or 0.01 M HCl. After treatment, the solutions were filtered, and the lithium-ion concentrations were analyzed via ICP-OES (Perkin Elmer).

Adsorption kinetics

Kinetics experiments were performed with resin **11** (50 mg) in 10 mL of 20 ppm Li^+ solution (pH: 7.0, 23 °C). The supernatant at adsorption times of 5, 15, 30 and 60 min was analyzed via ICP-OES. The q_t at various times was calculated via Eq. (1).[30,35]

Adsorption isotherms

Effect of initial Li^+ concentration (C_o)

Several experiments were carried out by stirring resin **11** (50 mg) in a Li^+ solution (10 mL, pH = 7.0, T = 23 °C) with lithium-ion C_o concentrations of 20, 40, 60, 80 and 100 ppm for 30 min. The q_t values were calculated via Eq. (1).[30,36]

Effect of adsorbent amount
Adsorption experiments were conducted with various doses (25, 50, 75 and 100 mg) of resin **11** in Li^+ solution (10 mL, 20 ppm, pH = 7.0, T = 23 °C). The supernatant at an adsorption time of 30 min was analyzed *via* ICP–OES to obtain q_t *via* Eq. (1).[30,36]

Effect of pH
The q_e values at various pH values (3, 5, 7 and 9) (30 min, T = 23 °C) for adsorption were determined using resin **11** (50 mg), 20 ppm Li^+ solution (10 mL) and Eq. (1).[30,36]

Selective adsorption
The competitive ions Na^+, K^+ and Mg^{2+} were examined to determine the recognition selectivity of resin **11** (50 mg) for Li^+. Adsorption experiments involving binary mixtures (10 mL, pH = 7.0) of Li^+/Na^+, Li^+/K^+ and Li^+/Mg^{2+} pairs with 20 ppm concentrations of each ion were performed at 23 °C for 30 min. Another experiment was carried out using a solution containing Li^+ (20 ppm) and Mg^{2+} (40 ppm). After the q_e and C_e values of the various ions were determined, the distribution coefficient K_d (L g^{-1}) was calculated *via* Eq. (3):[37,38]

$$K_d = \frac{q_e}{C_e} \tag{3}$$

The selectivity coefficient *k* of resin **11** toward Li^+ versus the competitive ion M^{n+} was determined via Eq. (4):[37,38]

$$k = \frac{K_{d(Li^+)}}{K_{d(M^{n+})}} \tag{4}$$

Regeneration: adsorption/desorption
Resin **11** (50 mg) was stirred with a 20 ppm Li^+ solution (10 mL) for 30 min to determine q_e. Then, the Li^+-resin **11** complex was placed in 0.5 M HCl (5 mL) for 30 min at 45 °C. The desorption efficiency was determined by analyzing the supernatants. The cycle was repeated five times.

Results
Synthesis and characterization of monomer 6, polymers 7 and 8, and resins 10 and 11
Before we proceeded to synthesize cross-linked resins **10** and **11**, a feasibility study was essential to synthesize linear polymers **7** and **8**. The successful synthesis of the linear polymers paved the way for the generation of resins **10** and **11**. Resin **11** was chosen for the adsorption study involving Li^+ ions since it was obtained in excellent yield (*vide infra*).

CE **1** was converted to its tosylate derivative **3** which was exposed to substitution of the tosyl group with diallyl amine **4** to produce 2-(diallylaminomethyl)–12-crown-4-ether (**5**) in very good yield (Scheme 1). Upon treatment with 1 equivalent of HCl, tertiary amine **5** afforded amine salt monomer **6** in almost quantitative yield (Scheme 1).

The NMR spectra of **1**, **3**, and **5** are displayed in Figs. 1 and 2. Owing to a chiral center at the carbon marked 'e', two Hs attached to each carbon at 'c' and 'd' in **5** become diastereotopic. As a result, CH_2 protons (CH_AH_M) are split into an AM doublet whereby each signal is further split into doublets owing to the presence of an adjacent H_X to give signals of AMX pattern as a doublet of doublets (Fig. 1c). The protons marked 'a' and 'b' appeared in the olefinic region. The ^{13}C spectrum of **5** in Fig. 2c displays the usual chemical shifts for the alkene carbons along with the chemical shifts for the remaining carbons, confirming the structure of tertiary amine **5**.

As outlined in Scheme 2, monomer **6** underwent APS-initiated cyclopolymerization, affording homopolymer **7**, whereas AIBN-initiated copolymerization of **6** with SO_2 led to alternate copolymer **8**. Reactivity ratios of $r_1 \approx 0$ and $r_2 \approx 0$ for the diallylamine salt/SO_2 pair dictate the formation of the alternate copolymer[39,40].

The NMR spectra of **6**–**8** are displayed in Figs. 3 and 4. Note that the two allyl groups are diastereotopic in nature, and as such, they become magnetically non-equivalent, which leads to separate signals of equal intensity for each carbon marked 'a', 'b', and 'c' (see the expanded spectrum in the inset (Fig. 4 a) in the range ~ δ125-127 ppm). The alkene proton signals at δ5.3 and 5.9 ppm (Fig. 3a) disappeared in the polymer spectra (Fig. 3b, c), confirming the formation of the polymers. Likewise, the alkene carbon signals marked 'a' and 'b' (Fig. 4a) were not present in the polymer spectra (Fig. 4b, c). The absence of residual alkene signals points towards the involvement of chain transfer to the monomer[41] and coupling[42] in the termination process. The major and minor signals for the carbons marked '**a**' and '**b**' are attributed to the substituents in the *cis*- and *trans*- dispositions in an approximate ratio of 3:1 (Fig. 4c)[43,44].

As outlined in Scheme 3, a solution of **6** (85 mol%) and cross-linker **9** (15 mol%) underwent APS-initiated polymerization to yield water-insoluble copolymeric resin **10**, whereas AIBN-initiated terpolymerization of **6**/**9**/SO_2 in an 85:15:115 mol ratio afforded cross-linked water-insoluble terpolymeric resin **11**. Compared with copolymer **10**, terpolymer **11** was obtained in better yield.

If monomers **6** and **9** exhibit equal reactivity, their feed ratio is expected to be reflected in the polymer composition at high conversion. In polymers **10** and **11**, the amine salt monomers are distributed randomly throughout the network, whereas in polymer **11**, the SO_2 units are incorporated in an alternating sequence.

Viscosity measurements
The viscosity plots for the PEs, displayed in Fig. 5, become concave upward, as expected, in salt-free water, whereas the plots become linear in 0.1 M NaCl since Cl^- ions shield the positive charges on the macromolecules.

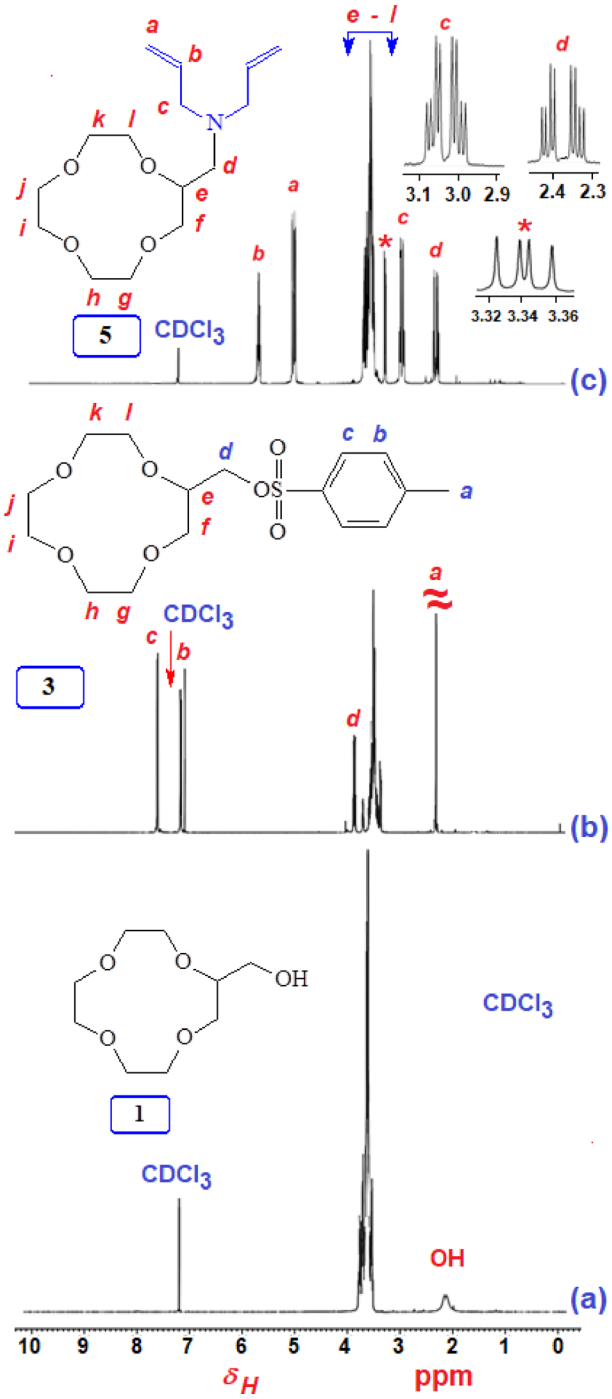

Fig. 1. ^{1}H spectra in $CDCl_3$ of (**a**) CE **1**, (**b**) tosylate derivative **3**, and (**c**) diallyl methyl-12-crown-4-ether amine **5**.

The respective intrinsic viscosities [η] of **7** and **8**, as determined via the relationship $\eta_{sp}/C = [\eta] + k\,[\eta^2 C]$, were 0.0661 and 0.261 dL g^{-1}, respectively. The low [η] value for homopolymer **7** is indicative of its lower molar mass. GPC analysis did not provide acceptable molar masses for the polymers; erratic results were obtained, presumably owing to the crown ether motifs being attached to the column materials.

TGA of cyclopolymers 8, 9, 10, and 11

The TGA curves (Fig. 6) revealed that polymers **8** and **9** and resins **10** and **11** are stable up to 200 °C. The weight loss for **9** and **11** occurring in the range 220–280 °C is accounted for the loss of SO_2 motifs, whereas in their absence, polymers **8** and **10** were more stable.

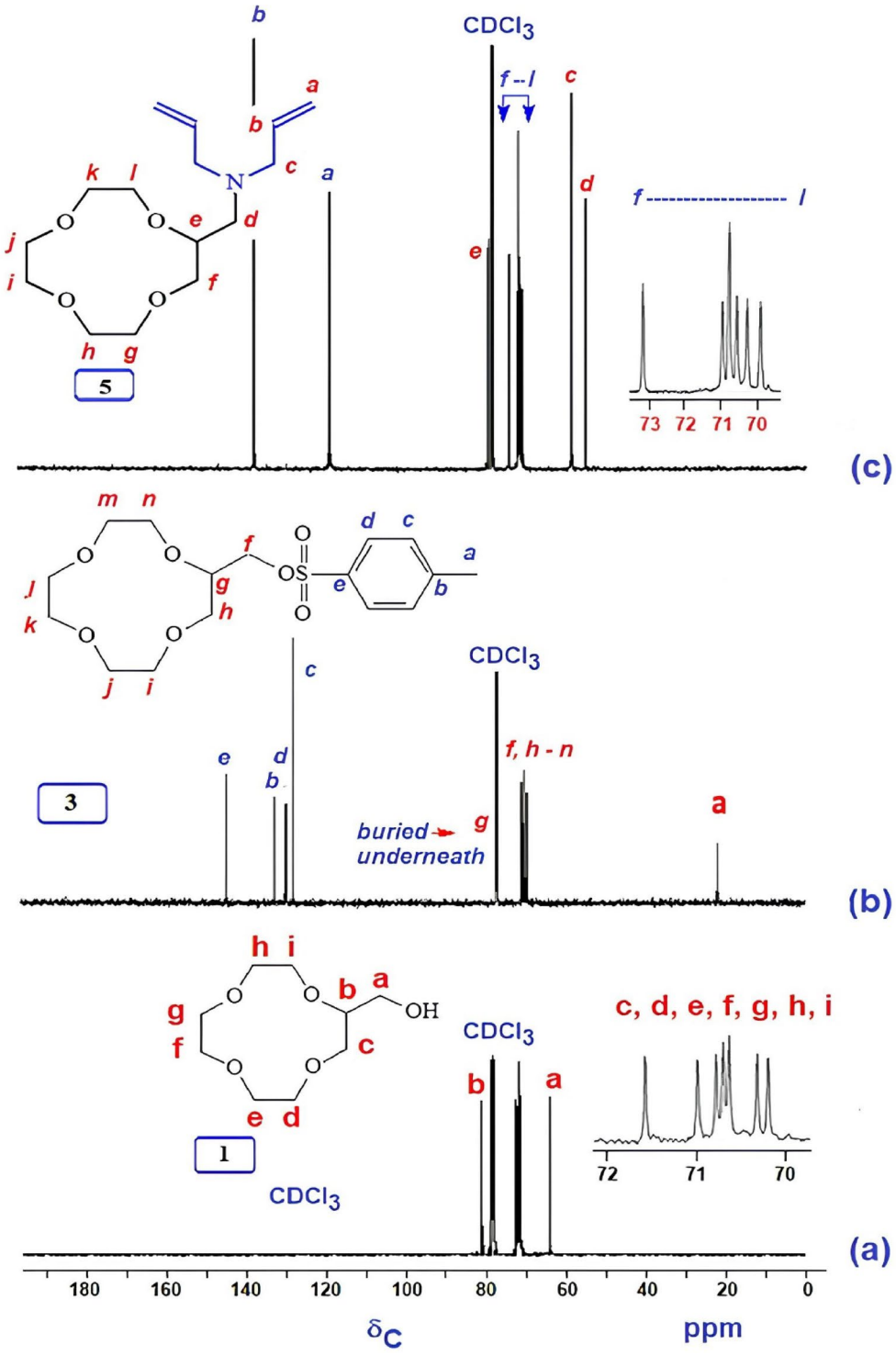

Fig. 2. ^{13}C spectra of (**a**) CE **1**, (**b**) tosylate derivative **3**, and (**c**) diallyl methyl-12-crown-4-ether amine **5** in $CDCl_3$.

FTIR analysis

The FTIR spectra of unloaded and lithium-loaded resin **11** are displayed in Fig. 7. The symmetric and asymmetric stretching bands of SO_2 appeared at ~1120 and 1305 cm^{-1}, respectively. There was a perceptible change in the vibration band of the crown ether C-O-C at approximately 1000–1100 cm^{-1}. A new band at 917 cm^{-1} is assigned to the complex of Li^+ ions with ether motifs[45].

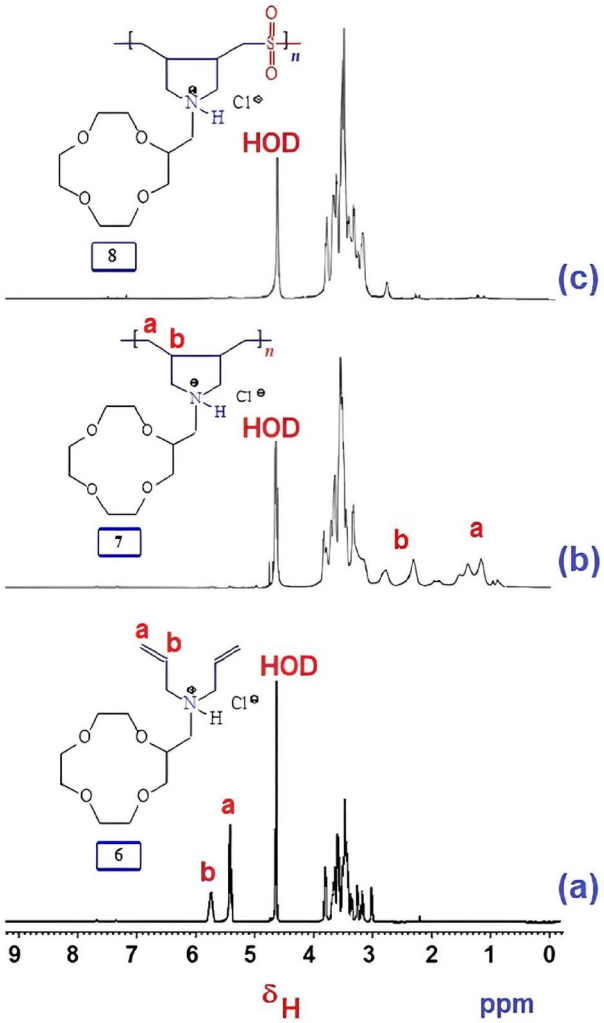

Fig. 3. ^{1}H spectra of (**a**) monomer **6**, (**b**) homopolymer **7**, and (**c**) the copolymer with SO_2**8**.

BET analyses of cross-linked resin 11

The textural properties of CLR **11** were determined through BET analysis (Table 1 ; Fig. 8 a). The material exhibited a significantly greater surface area (410.47 m^2/g) than conventional ionic resins[46,47]. This increased surface area is likely due to the expanded morphology resulting from the incorporation of crown ether moieties. Desorption isotherms were analyzed via the BJH method to determine the pore size distribution of the resin (Fig. 8 b). Average pore diameter of 2.9 nm reflects mesoporous nature of resin **11**.

SEM and EDX analysis

The surface morphology of unloaded and metal-ion-loaded resin **11** was examined by SEM after gold coating. The unloaded resin exhibited a smooth surface with flat crystalline structures. In contrast, the loaded resin showed noticeable changes in surface roughness and morphology, indicating the deposition of metal ions. EDX analysis confirmed the presence of C, O, N, Cl, and S, which is consistent with the composition of resin **11**. However, in the case of the Li^+-loaded resin, lithium was not detected in the EDX spectrum alongside C, O, S, and N. This is likely because lithium is difficult to detect via EDX because of several factors, such as its low atomic number, which emits X-rays with very low energy (approximately 54 eV), weak characteristic X-ray emission, and the limited sensitivity of Detectors for elements lighter than boron. The Decrease in chloride ions in the loaded sample resulted from the adjustment of the pH to 7 with NH_4OH, whereby Cl^- ions may have been leached out as NH_4Cl. The morphology changes suggest the adsorption of Li^+ ions on resin **11** (Fig. 9)[48,49]. The EDX analysis is not known to detect Li; conventional EDX detectors are optimized for elements with atomic number ≥ 4.

XPS analysis

The XPS survey scan for the unloaded and loaded resin **11** compositions revealed the presence of carbon, oxygen, sulfur and nitrogen atoms within the resin surface structure, having highest percentage of carbon contents (Tables 2 and 3; Figs. 10 a5 and b5). The XPS deconvoluted profiles of the **C 1s** spectrum for unloaded resin **11**

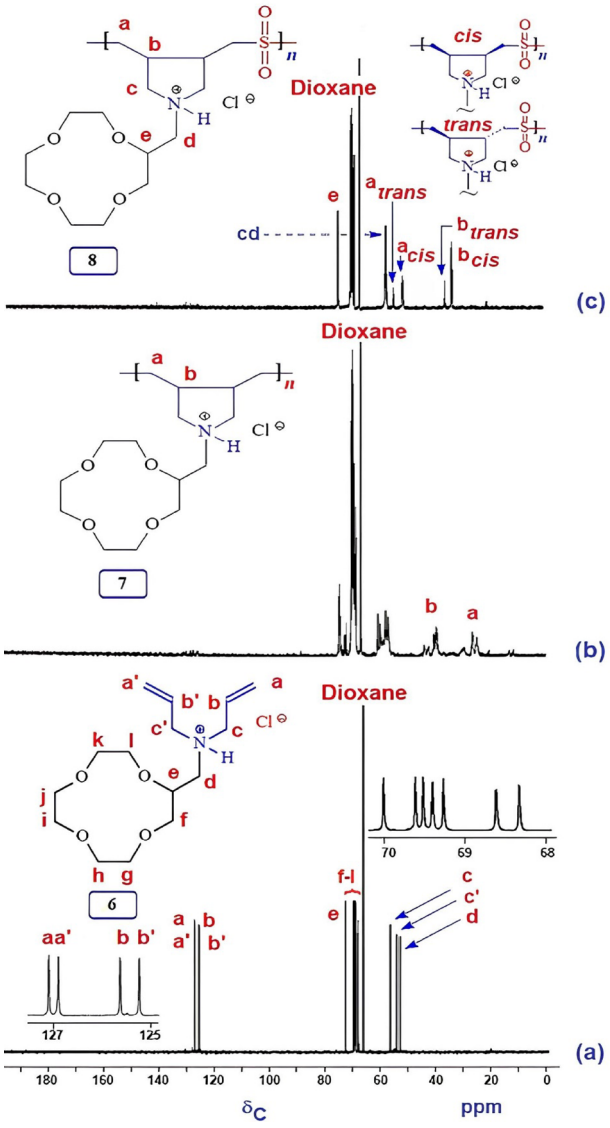

Fig. 4. ^{13}C spectra of (**a**) Monomer **6**, (**b**) homopolymer **7** and (**c**) the copolymer with SO_2**8**.

showed a two-peak profile (Fig. 10a1); the less intense peak at 284.76 eV was attributed to C–C Aliphatic bonds, whereas the intense peak at 286.24 eV indicated the presence of C–O, C–S and C–N bonds. For the loaded resin **11**, the C 1 s spectrum showed two peaks, like the unloaded sample, but the only difference was the Decreased intensity of the peak at 285.87 cm^{-1} (Fig. 10b1).

The presence of O 1 s peaks for the unloaded resin **11** at 532.46, 532.41 and 531.98 eV were attributed to O = S, O–C and O_2, respectively, whereas the loaded resin **11** had the same three peaks with approximately the same binding Energy in the range of 531–533 eV (Fig. 10a2 and b2). The XPS spectrum of N 1 s for unloaded resin **11** presented two peaks related to the C-N bond; the less intense peak at 399.25 eV and the highly intense peak at 401.97 eV were indicative of the presence of trivalent unprotonated and quaternary protonated nitrogen (Fig. 10 a3 and b3). On the other hand, loaded resin **11** showed the opposite trend in intensity. The S 2p XPS spectra of the unloaded and loaded resins **11** were similar, as both had two peaks at 168.31, 169.37 eV attributed to S = O and S-C bonds (Fig. 10a4 and b4). Unfortunately, the presence of Li^+ ions was not detected in loaded resin **11**, where the initial concentration before adsorption was 20 ppm[50,51]. The determination of low content Li^+ using XPS was either difficult or inaccurate[50].

Discussion

Adsorption

In a simplified form, the process of Li^+ extraction from its aqueous solution into the solid phase of the resin can be described as follows:

$$CE_s + Li^+_{aq} + Cl^-_{aq} \rightleftharpoons CE \cdot LiCl_{suspended}.$$

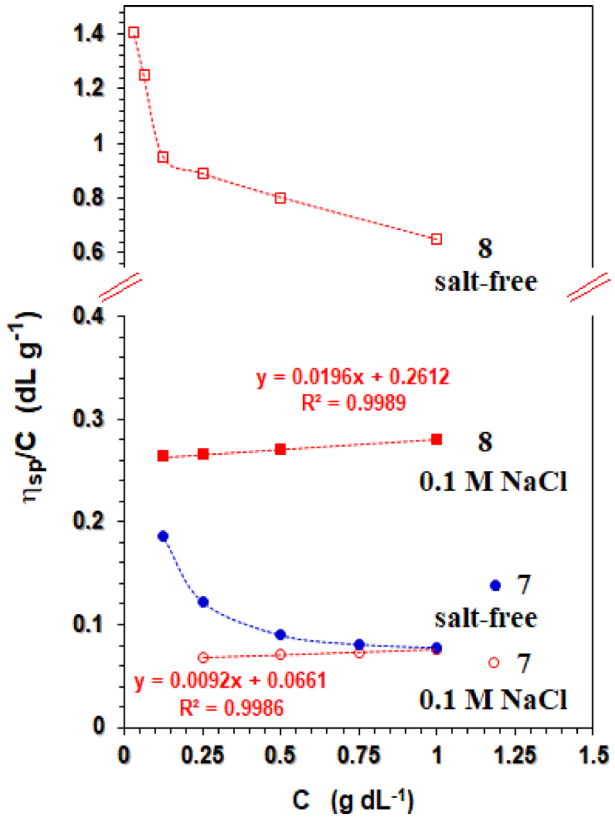

Fig. 5. Viscosity plots of **7** and **8** at 30 °C.

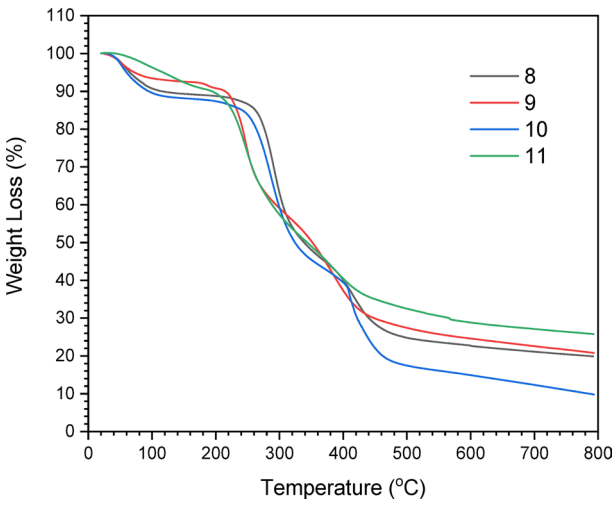

Fig. 6. TGA results for homopolymer **8**, SO_2 copolymer **9**, resin **10** and SO_2 resin **11**.

The equilibrium concentration (C_e) and adsorption capacity (q_e) were calculated *via* Eq. (1) (Table 4) for resin **11**, with initial lithium concentrations (C_o) ranging from 20 to 100 ppm at pH 7.0, for a Duration of 60 min at 23 °C. The percentage of lithium removal efficiency (E%) by resin **11** was determined *via* Eq. (2). For a solution of 20 ppm Li^+ at various pH values, the plot of q_e versus pH (Fig. 11a) reveals the maximum adsorption capacity at pH 7; at lower pH values, competition between H^+ and Li^+ lowers the q_e for Li^+ ions. Therefore, the subsequent experiments were performed at pH 7. A linear relationship between C_o and q_e is illustrated in Fig. 11b. The q_e values rose up with increasing C_o, whereas the removal percentage decreased at higher concentrations since the adsorption sites were saturated with Li^+ ions with no further available vacant sites (Table 4).

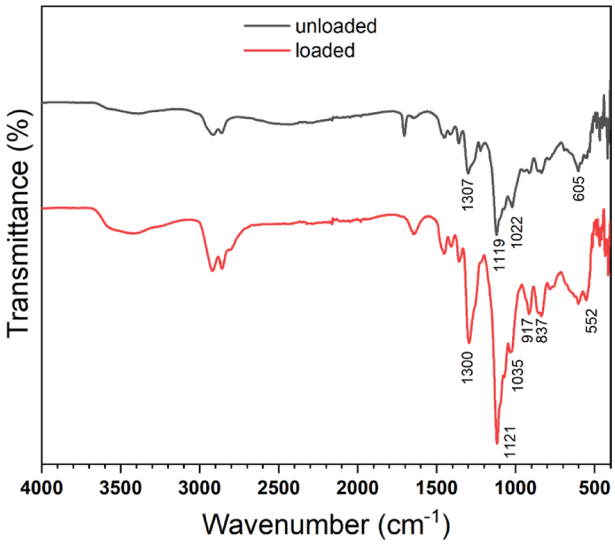

Fig. 7. FTIR spectra of unloaded and loaded cross-linked polymer **11** with lithium ions.

Parameters	Values
BET surface area	410.47 m^2g^{-1}
Total pore volume (at $P/P_0 \approx 0.98$)	0.30 cm^3g^{-1}
Average pore diameter	2.9 nm

Table 1. BET surface area analysis of cross-linked resin **11.**

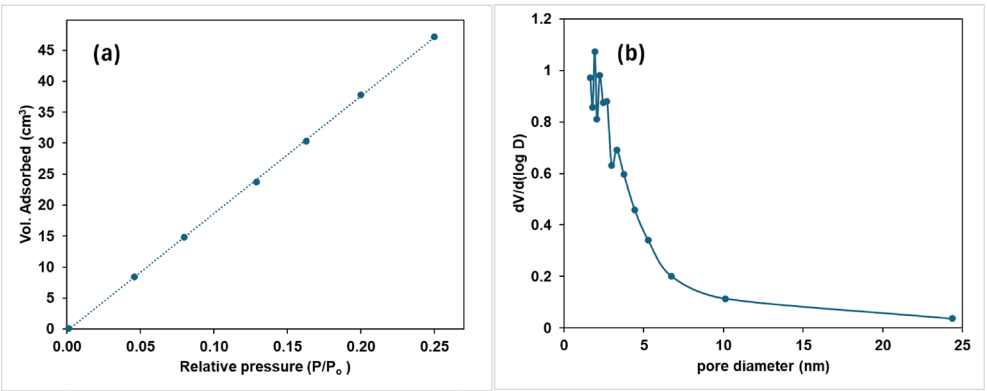

Fig. 8. For resin **11**, **(a)** nitrogen adsorption–desorption isotherms and **(b)** pore size distributions as determined via the BJH method.

Kinetic studies and isotherms of lithium adsorption

The adsorption mechanism can be illustrated by analyzing the relationship between C_e and q_e. This relationship is established *via* adsorption isotherm models, which help describe the formation of adsorbate layers on the adsorption sites, the characteristics of these sites, and the nature of the interactions involved[52]. In this study, several isotherm models were applied to interpret adsorption behavior.

To determine the homogeneity and heterogeneity of the adsorption of lithium ions on a surface with uniform energy, the Langmuir and Freundlich isotherm models (Eqs. (5) and (6), respectively) were used. Linear plots for the Langmuir model and Freundlich isotherm were constructed (Fig. 12a, b, respectively). The constants q_m and K_L for the Langmuir isotherm and n and K_f for the Freundlich isotherm can be calculated from the graphs (Table 5). The adsorption intensity or heterogeneity factor (**n**) value ($n = 2.84 > 1$) indicates that favorable selective adsorption occurred primarily through a chemisorption mechanism[53] and increased with increasing metal ion concentration but at a decreasing rate. The maximum adsorption q_m was Determined to be 4.98 mg g^{-1}. Heterogeneous surfaces of porous materials have been detailed in a review article[54]. Adsorption isotherms can

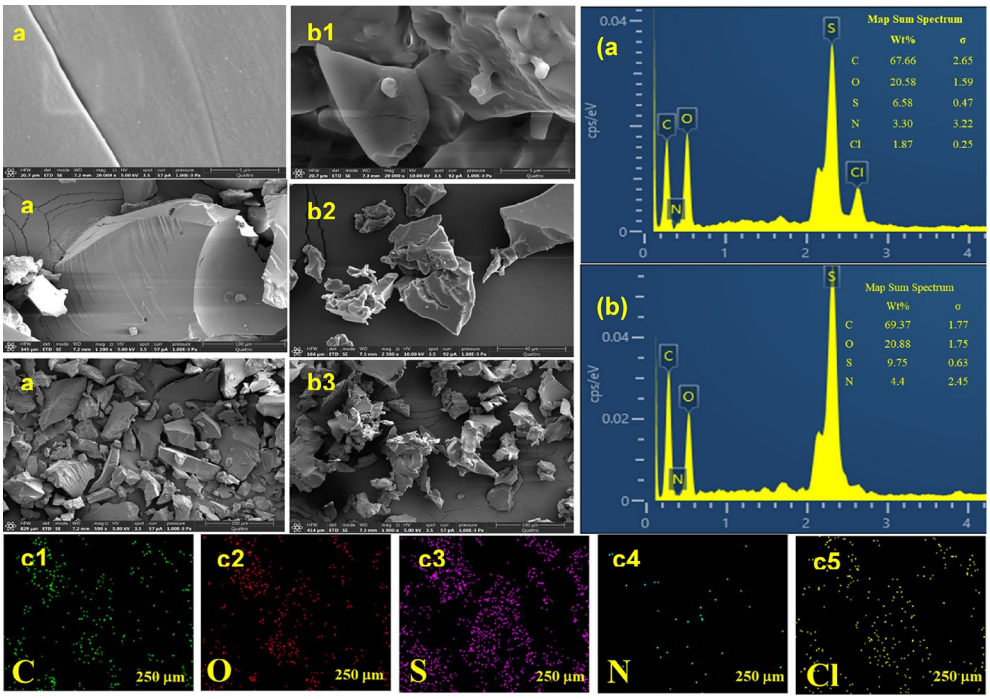

Fig. 9. SEM and EDX analysis of (**a**) unloaded **11**, (**b**) Li^+-loaded **11**, and (**c**) elemental mapping images of unloaded **11**.

Name	Peak BE	FWHM eV	Atomic %
C1s A	286.24	1.94	42.64
C1s B	284.76	1.43	21.84
O1s A	532.46	2.6	16.3
O1s B	532.41	1.35	10.51
O1s C	531.98	0.91	1.17
N1s A	401.97	1.86	2.12
N1s B	399.25	1.63	0.68
S2p3 A	168.31	1.93	3.15
S2p1 A	169.37	1.93	1.58

Table 2. XPS survey scan composition of the unloaded resin **11.**

Name	Peak BE	FWHM eV	Atomic %
C1s A	285.87	2.28	64.94
C1s B	286.72	0.83	23.6
O1s A	530.59	1.73	0.79
O1s B	532.85	2.56	8.45
O1s C	532.43	1.63	15.07
N1s A	399.25	1.48	2.63
N1s B	401.81	2.33	1.43
S2p3 A	168.26	1.8	3.35
S2p1 A	169.32	1.8	1.64

Table 3. XPS survey scan composition of Li^+-loaded resin **11**.

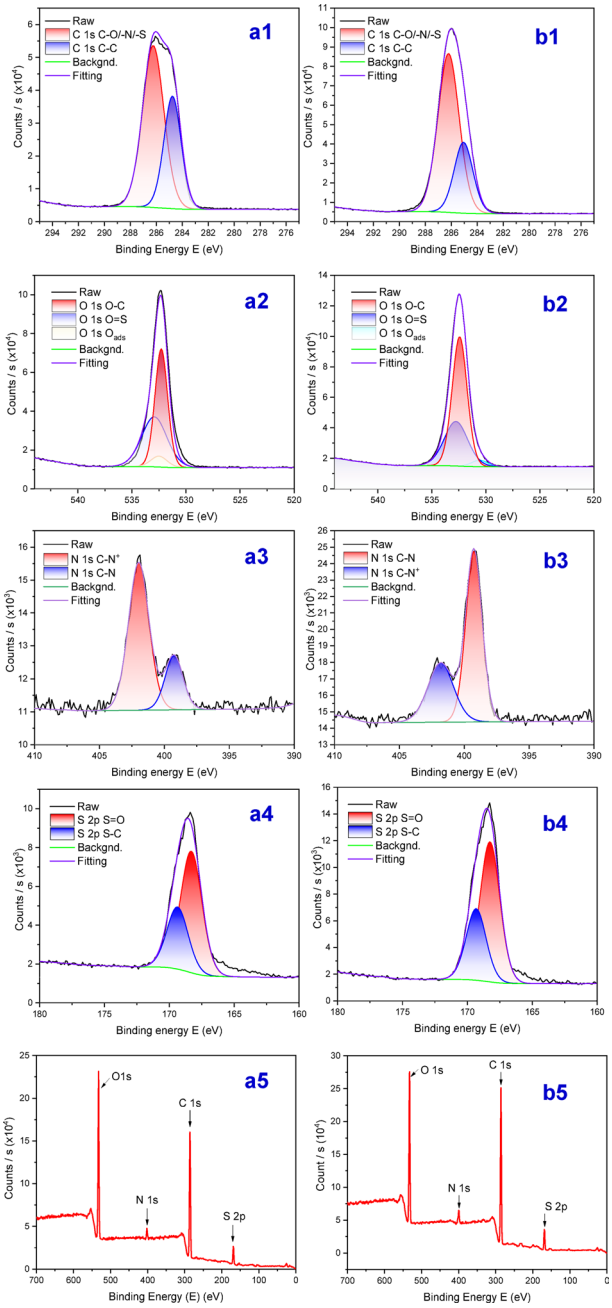

Fig. 10. XPS analysis of (**a**) unloaded resin **11** and (**b**) Li^+-loaded resin **11**.

C_o (mg L^{-1})	C_e (mg L^{-1})	q_e (mg g^{-1})	Removal (%)
20	9.99	2.00	50.1
40	26.2	2.76	34.5
60	43.3	3.34	27.8
80	61.4	3.72	23.3
100	79.1	4.18	20.9

Table 4. C_e, q_e and E% values of lithium adsorption.

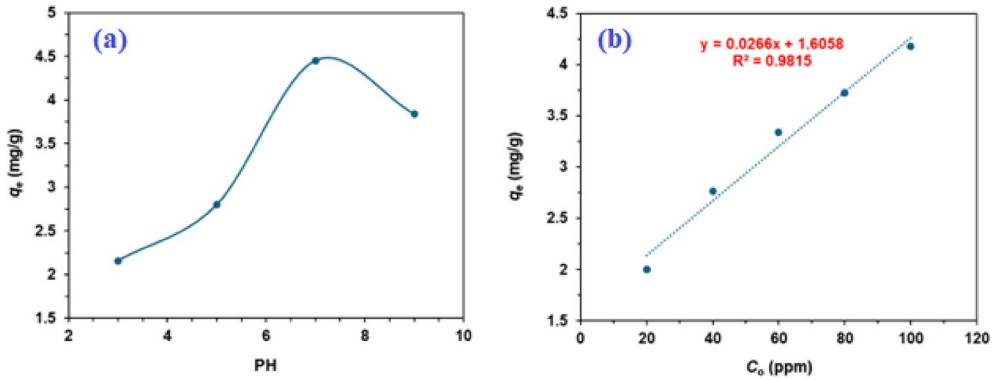

Fig. 11. Plots for **(a)** q_e *versus* various pH values for a constant C_o (20 ppm Li^+), **(b)** q_e *versus* C_0.

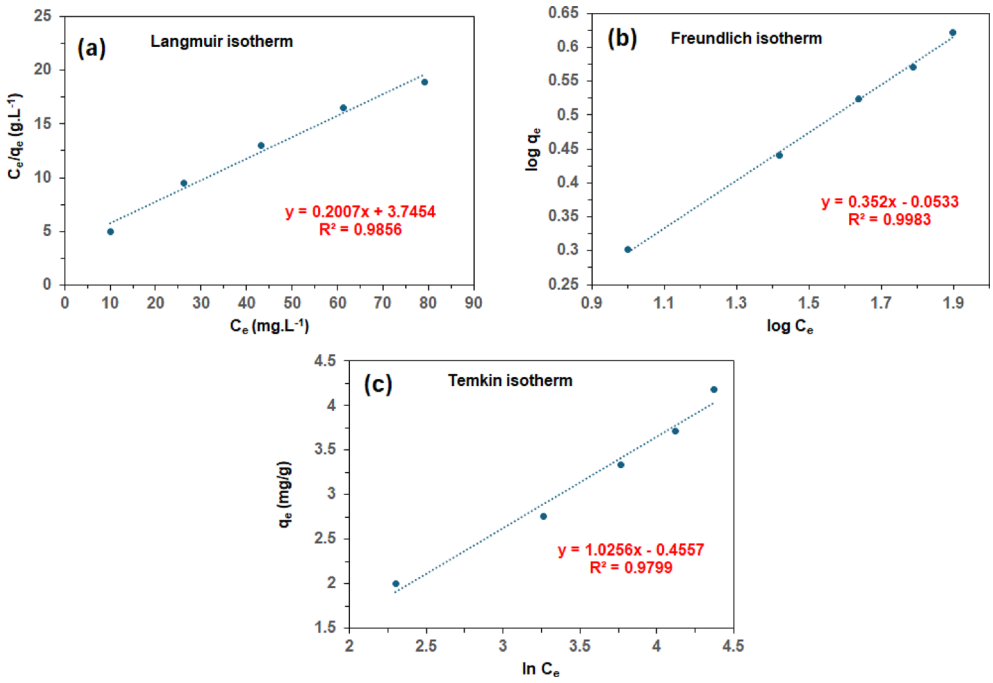

Fig. 12. (**a**) Langmuir, (**b**) Freundlich and (**c**) Temkin isothermal models for lithium adsorption using resin **11** at 23 °C.

Langmuir		
q_m (mg g^{-1})	**K_L or b (L. mg^{-1})**	***R*²**
4.98	0.05	0.9856
Freundlich		
n	**K_f ($mg^{1-1/n}$ g^{-1} $L^{1/n}$)**	***R*²**
2.84	0.885	0.9983
Temkin		
B	**A**	***R*²**
1.026	0.641	0.9799

Table 5. Isotherm constants for lithium adsorption on resin **11** at 23 °C.

shed light on the heterogeneity of the surfaces. For instance, based on Freundlich isotherm model, if $0 < 1/n < 1$, the adsorption is considered favorable, and the surface is heterogeneous. Freundlich constant n of 2.84 thereby points towards the heterogeneity of the adsorbent surface[55]. A highly heterogeneous surface is indicated If 1/n approaches 0, whereas 1/n approaching 1 the surface becomes closer to homogeneous. A more heterogeneous surface with a smaller value of n signifies a wider distribution of adsorption site energies, where stronger binding occurs to more energetic sites initially. This is observed with initial faster followed by slow adsorption (*vide infra* Fig. 13a).

$$Langmuir\ isotherm\ model: \frac{C_e}{q_e} = \frac{1}{q_m}C_e + \frac{1}{K_L q_m} \tag{5}$$

$$Fruendlich\ isotherm\ model: \log q_e = log k_f + \frac{1}{n}\, log C_e \tag{6}$$

For a uniform distribution of binding sites, the Temkin isotherm describes the interaction between the adsorbent and adsorbate[56]. A linear plot of q_e versus ln (C_e) was generated (Fig. 12 c), where the binding constant (**A**) and heat of adsorption (**B**) were obtained from the respective intercept and slope, as defined by Eq. (7) (Table 5). The Temkin isotherm provided a good fit for lithium adsorption, indicating that its adsorption is influenced by surface coverage resulting from specific interactions between the adsorbate and the adsorbent.

$$Temkin\ isotherm\ model: q_e = \frac{RT}{b}\, lnA + \frac{RT}{b}\, ln\, C_e = BlnA + Bln\, C_e \tag{7}$$

The kinetic behavior of the adsorptions was studied via pseudo first- and second-order linear equations (Eqs. 8 and 9)[57].

$$pseudo\ first\ order\ kinetic: \ln(q_e - q_t) = ln\, q_e - k_1 t \tag{8}$$

$$pseudo\ second\ order\ kinetic: \frac{t}{q_t} = \frac{1}{k_2 q_e^2} + \frac{t}{q_e} \tag{9}$$

where the rate constants k_1 (min^{-1}) and k_2 ($g{\cdot}mg^{-1}{\cdot}min^{-1}$) correspond to the respective first- and second-order kinetic models. The q_t and C_t values were determined at various times. The uptake of Li^+ ions by **11** reached 50% within 5 min (Fig. 13a). The pseudo-second-order model indicated a better fit (Fig. 13b vs. Figure 13c); k_2 was found to be 0.351 g mg^{-1} min^{-1} (Table 6).

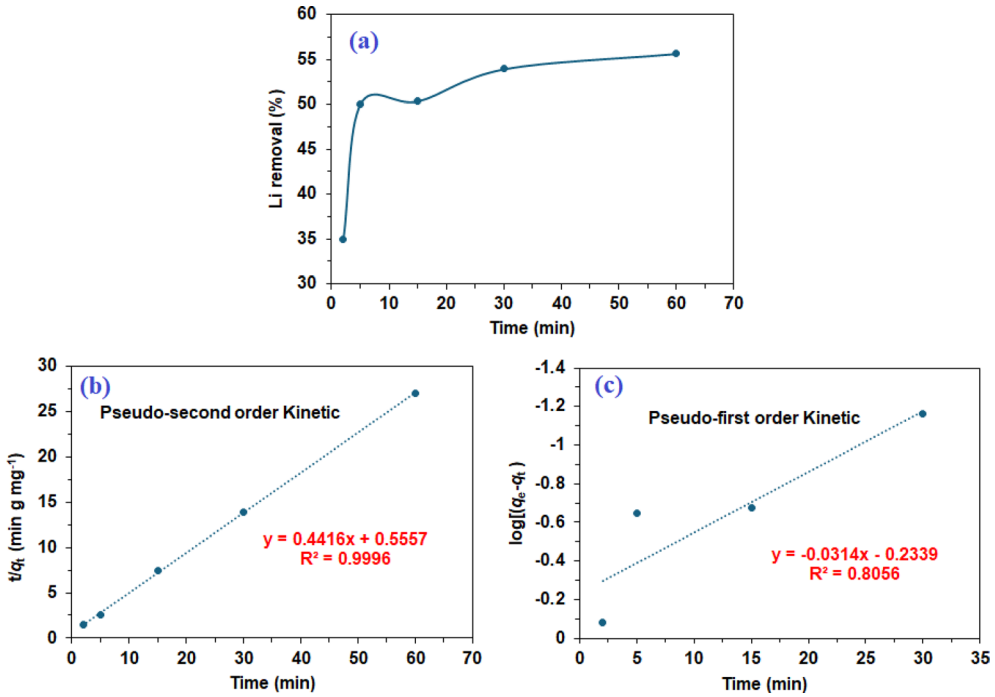

Fig. 13. Kinetic behavior of lithium adsorption by resin **11** at 23 °C: **(a)** plot of time versus removal percentage (C_o = 20 ppm), **(b)** pseudo-first order and **(c)** pseudo-second order kinetic graphs.

Second-order kinetics				
q_{e_Calc}(mg g^{-1})	k_2(g mg^{-1}min^{-1})	q_{e_Exp}(mg g^{-1})	h^a(min^{-1}mg g^{-1})	R^2
2.264	0.351	2.226	1.8	0.9996

Table 6. Constant values of second-order kinetics for lithium adsorption at 23 °C on resin **11.**

Entry	Ion pair	C_0 (mg L^{-1})	Volume (mL)	C_e (mg L^{-1})	q_e mg g^{-1}	K_d[a] (L g^{-1})	k [b]
1	Li^+	20	10	12.6	1.48	0.117	—very high[c]
	Na^+	20	10	20	≈0	≈0	
2	Li^+	20	10	12.3	1.54	0.125	— very high[c]
	K^+	20	10	20	≈0	≈0	
3	Li^+	20	10	13.1	1.38	0.105	1.53
	Mg^{2+}	20	10	14.9	1.02	0.0685	
4	Li^+	20	10	15.6	0.882	0.056	0.533
	Mg^{2+}	40	10	29.7	2.07	0.105	

Table 7. Distribution and selectivity coefficient for the adsorption of several ion pairs. [a]distribution coefficient (Eq. (3)). [b]selectivity coefficient (Eq. (4)). [c]Not Determined since q_e is ≈0.

Selectivity

Li^+ selectivity was evaluated against Na^+, K^+ and Mg^{2+} contents. Table 7 shows the results of the adsorption of various ions by CLR **11**. The respective adsorption capacities (q_e) of CLR **11** for Li^+, Na^+ and K^+ and Mg^{2+} (20 mg L^{-1} for each M^{n+}, pH = 7.0) reached 1.38–1.54, 0, 0 and 1.02 mg g^{-1}, respectively (entries 1–3, Table 7). The higher q_e for Li^+ on CLR **11** than for the other ions is because of the cavity size of the 12-crown-4 ether motif. The cavity radius of ~ 75 pm for 12-crown-4 matches the ionic radius of Li^+ (76 pm), whereas the sizes of Na^+, K^+ and Mg^{2+} are 102, 138 and 72 pm, respectively[58,59]. The ionic size of Mg^{2+} is nearly the same as Li^+ ions. The selectivity coefficients k of CLR **11** for Li^+ with respect to the competing ions Na^+, K^+, and Mg^2 are >>1, >> 1, and 1.53, respectively. Note the selectivity coefficient $k = \frac{K_{d(Li+)}}{K_{d(M^{n+})}}$ from a solution containing 20 ppm each of Li^+ and Mg^{2+} is 1.533, whereas it became 0.533 from a solution containing 20 ppm Li^+ and 40 ppm Mg^{2+} (entry 4, Table 7). The adsorbent is more selective to Li^+ than Mg^{2+} from a solution containing equal concentrations (i.e. 20 ppm each), whereas k changes in favor of Mg^{2+} from a solution containing its higher concentration.

Regeneration

Li^+ from the adsorbent **11**-Li^+ complex was Desorbed using 0.5 M HCl. After 5 cycles, q_e retained 89% of its original value, thereby suggesting preservation of the structural integrity and binding sites for Li^+.

Conclusion

Homopolymer **7**, copolymer **8**, and CLR **10** were synthesized *via* the cyclopolymerization of monomer **6**. The new adsorbent **11** was synthesized via the polymerization of a diallyl amine salt monomer bearing 12-crown-4 ether motif, SO_2, and cross-linker **9**. The lithium removal study was conducted at ppm level. Resin **11** adsorbs lithium ions rapidly with excellent efficiency following second-order kinetics and fitting the Temkin and Langmuir adsorption isotherms. The extraction efficiency of resin **11** for the selective adsorption of Li^+ versus Na^+, K^+, and Mg^{2+} was evaluated, and the selectivity coefficient k was found to be >>1, >> 1, and 1.54, respectively. These results show that CLR **11** selectively recognizes the target ion Li^+.

Data availability

The datasets used and/or analysed during the current study are available from the corresponding author on reasonable request.

Received: 20 June 2025; Accepted: 4 September 2025
Published online: 07 October 2025

References

1. Shen, Y. Recycling cathode materials of spent lithium-ion batteries for advanced catalysts production. *J. Power Sources*. **528**, 231220. https://doi.org/10.1016/j.jpowsour.2022.231220 (2022).
2. Xiao, J., Li, J. & Xu, Z. Challenges to future development of spent lithium ion batteries recovery from environmental and technological perspectives. *Environ. Sci. Technol.* **54**, 9–25. https://doi.org/10.1021/acs.est.9b03725 (2020).
3. Tarascon, J. M. & Armand, M. Issues and challenges facing rechargeable lithium batteries. *Nature* **414**, 359–367. https://doi.org/10.1038/35104644 (2001).
4. Fu, Nitta, N., Wu, F., Lee, J. T. & Yushin, G. Li-ion battery materials: present and future. *Mater. Today*. **18**, 252–264. https://doi.org/10.1016/j.mattod.2014.10.040 (2015).

5. Choi, J. W. & Aurbach, D. Promise and reality of post-lithium-ion batteries with high energy densities. *Nat. Rev. Mater.* **1**, 16013. https://doi.org/10.1038/natrevmats.2016.13 (2016).
6. Mukhopadhyay, A. & Jangid, M. K. Li metal battery, heal thyself. *Science* **359**, 1463. https://doi.org/10.1126/science.aat2452 (2018).
7. Makuza, B., Tian, Q., Guo, X., Chattopadhyay, K. & Yu, D. Pyrometallurgical options for recycling spent lithium-ion batteries: a comprehensive review. *J. Power Sources*. **491**, 229622. https://doi.org/10.1016/j.jpowsour.2021.229622 (2021).
8. Niese, N., Pieper, C., Arora, A. & Xie, A. *The Case for a Circular Economy in Electric Vehicle Batteries* (Preprint at The Case for a Circular Economy in Electric Vehicle Batteries | BCG, 2020).
9. Energy, N. Recycle spent batteries. *Nat. Energy*. **4**, 253. https://doi.org/10.1038/s41560-019-0376-4 (2019).
10. Zeng, X., Li, J. & Liu, L. Solving spent lithium-ion battery problems in china: opportunities and challenges. *Renew. Sustain. Energy Rev.* **52**, 1759–1767. https://doi.org/10.1016/j.rser.2015.08.014 (2015).
11. Tran, M. K., Rodrigues, M. T., Kato, K., Babu, G. & Ajayan, P. M. Deep eutectic solvents for cathode recycling of Li-ion batteries. *Nat. Energy*. **4**, 339–345. https://doi.org/10.1038/s41560-019-0368-4 (2019).
12. Zhou, L. F., Yang, D. R., Du, T., Gong, H. & Luo, W. B. The current process for the recycling of spent lithium ion batteries. *Front. Chem.* **8**, 578044. https://doi.org/10.3389/fchem.2020.578044 (2020).
13. Xiao, J. L., Sun, S. Y., Song, X., Li, P. & Yu, J. G. Lithium ion recovery from Brine using granulated polyacrylamide-MnO2 ion-sieve. *Chem. Eng. J.* **279**, 659–666. https://doi.org/10.1016/j.cej.2015.05.075 (2015).
14. Swain, B. Recovery and recycling of lithium: A review. *Sep. Purif. Technol.* **172**, 388–403. https://doi.org/10.1016/j.seppur.2016.08.031 (2017).
15. Shin, S. M., Kim, N. H., Sohn, J. S., Yang, D. H. & Kim, Y. H. Development of a metal recovery process from Li-ion battery wastes. *Hydrometallurgy* **79**, 172–181. https://doi.org/10.1016/j.hydromet.2005.06.004 (2005).
16. Ferreira, D. A., Prados, L. M. Z., Majuste, D. & Mansur, M. B. Hydrometallurgical separation of aluminium, cobalt, copper and lithium from spent Li-ion batteries. *J. Power Sources*. **187**, 238–246. https://doi.org/10.1016/j.jpowsour.2008.10.077 (2009).
17. Liu, C. W., Lin, J., Cao, H. B., Zhang, Y. & Sun, Z. Recycling of spent lithium-ion batteries in view of lithium recovery: a critical review. *J. Clean. Prod.* **228**, 801–813. https://doi.org/10.1016/j.jclepro.2019.04.304 (2019).
18. McKnight, R. F. et al. Lithium toxicity profile: A systematic review and meta-analysis. *Lancet* **379**, 721–728. https://doi.org/10.1016/S0140-6736(11)61516-X (2012).
19. Park, M. J. et al. Recyclable composite nanofiber adsorbent for li++ recovery from seawater desalination retentate. *Chem. Eng. J.* **254**, 73–81. https://doi.org/10.1016/j.cej.2014.05.095 (2014).
20. Kanagasundaram, T., Murphy, O., Haji, M. N. & Wilson, J. J. The recovery and separation of lithium by using solvent extraction methods. *Coord. Chem. Rev.* **509**, 215727. https://doi.org/10.1016/j.ccr.2024.215727 (2024).
21. Steed, J. W. First- and second-sphere coordination chemistry of alkali metal crown ether complexes. *Coord. Chem. Rev.* **215**, 171–221. https://doi.org/10.1016/S0010-8545(01)00317-4 (2001).
22. Gokel, G. W., Leevy, W. M. & Weber, M. E. Crown ethers: sensors for ions and molecular scaffolds for materials and biological models. *Chem. Rev.* **104**, 2723–2750. https://doi.org/10.1021/cr020080k (2004).
23. Pedersen, C. J. Cyclic polyethers and their complexes with metal salts. *J. Am. Chem. Soc.* **89**, 7017–7036. https://doi.org/10.1021/ja01002a035 (1967).
24. Torrejos, R. E. C. et al. Liquid–liquid extraction of li++ using mixed carrier system at room temperature ionic liquid. *Desalin. Water Treat.* **53**, 2774–2781. https://doi.org/10.1080/19443994.2014.931534 (2015).
25. Swain, B. Separation and purification of lithium by solvent extraction and supported liquid membrane, analysis of their mechanism: a review. *J. Chem. Technol. Biotechnol.* **91**, 2549–2562. https://doi.org/10.1002/jctb.4976 (2016).
26. Zhou, W. et al. A green strategy for lithium isotopes separation by using mesoporous silica materials doped with ionic liquids and benzo-15-crown-5. *J. Radioanal Nucl. Chem.* **300**, 843–852. https://doi.org/10.1007/s10967-014-3052-y (2014).
27. Pei, H. et al. In situ one-pot formation of crown ether functionalized polysulfone membranes for highly efficient lithium isotope adsorptive separation. *Eur. Polym. J.* **109**, 288–296. https://doi.org/10.1016/j.eurpolymj.2018.10.001 (2018).
28. Hua, J. et al. A remarkable improved li++/Mg2+ selectivity and li++ recovery simultaneously by adding crown ether to tributyl phosphate-ionic liquid extraction system as co-extractant. *Sep. Purif. Technol.* **335**, 126162. https://doi.org/10.1016/j.seppur.2023.126162 (2024).
29. Luo, X. et al. Recovery of lithium from wastewater using development of Li ion-imprinted polymers. *Sustain. Chem. Eng.* **3**, 460–467. https://doi.org/10.1021/sc500659h (2015).
30. Liu, W. Extraction of lithium ions from acidic solution using electrochemically imprinted membrane. *Desalination* **496**, 114751. https://doi.org/10.1016/j.desal.2020.114751 (2020).
31. Butler, G. B. & Cyclopolymerization and cyclocopolymerization; Marcel Dekker: New York, (1992). https://doi.org/10.1201/9781003066828
32. Butler, G. B. & Cyclopolymerization. *J. Polym. Sci.* **38**, 3451–3461. https://doi.org/10.1002/1099-0518(20001001)38:19<3451::AID-POLA10>3.0.CO;2-N. (2000).
33. McGrew, F. C. Structure of synthetic high polymers. *J. Chem. Educ.* **35**, 178. https://doi.org/10.1021/ed035p178 (1958).
34. Ali, S. A., Mubarak, S. A., Yaagoob, I. Y., Arshad, Z. & Mazumder, M. A. J. A sorbent containing pH-responsive chelating residues of aspartic and maleic acids for mitigation of toxic metal ions, cationic, and anionic dyes. *RSC Adv.* **12**, 5938–5952. https://doi.org/10.1039/D1RA09234K (2022).
35. Buhani, Suharso, S. Adsorption kinetics and isotherm of Cd(II) ion on Nannochloropsis Sp biomass imprinted ionic polymer. *Desalination* **259**, 140–146. https://doi.org/10.1016/j.desal.2010.04.019 (2010).
36. Du, X. et al. A novel electroactive λ-MnO2/PPy/PSS core–shell Nanorod coated electrode for selective recovery of lithium ions at low concentration. *J. Mater. Chem. A*. **4**, 13989–13996. https://doi.org/10.1039/C6TA05985F (2016).
37. Liu, B. J., Wang, D. F., Li, H. Y., Xu, Y. & Zhang, L. As(III) removal from aqueous solution using α-Fe2O3 impregnated Chitosan beads with As(III) as imprinted ions. *Desalination* **272**, 286–292. https://doi.org/10.1016/j.desal.2011.01.034 (2011).
38. Singh, D. K. & Mishra, S. Synthesis and characterization of Hg(II)-ion-imprinted polymer: kinetic and isotherm studies. *Desalination* **257**, 177–183. https://doi.org/10.1016/j.desal.2010.02.026 (2010).
39. Aldahdooh, M. K. & Ali, S. A. Synthesis and application of alternate cyclopolymers of β-diallylaminoethyliminodiacetic acid with maleic acid and sulfur dioxide. *React. Funct. Polym.* **161**, 104857. https://doi.org/10.1016/j.reactfunctpolym.2021.104857 (2021).
40. Yaagoob, I. Y., Ali, S. A., Al-Muallem, H. A. & Mazumder, M. A. J. Scope of sulfur dioxide incorporation into alkyldiallylamine-maleic acid-SO2 tercyclopolymer. *RSC Adv.* **8**, 38891–38902. https://doi.org/10.1039/C8RA08723G (2018).
41. Butler, G. B. & Angelo, R. J. Preparation and polymerization of unsaturated quaternary ammonium compounds. VIII. A proposed alternating Intramolecular-intermolecular chain propagation. *J. Am. Chem. Soc.* **79**, 3128–3131. https://doi.org/10.1021/ja01569a037 (1957).
42. Pike, R. M. & Cohen, R. A. J. Polym. Sci. Organophosphorus polymers. I. Peroxide-initiated polymerization of diethyl and diisopropyl vinylphosphonate. *J. Polym. Sci.* **44**, 531–538. https://doi.org/10.1002/pol.1960.1204414424 (1960).
43. Ali, S. A., Rasheed, A. & Wazeer, M. I. M. Synthesis and solution properties of a quaternary ammonium polyampholyte. *Polymer* **40**, 2439–2446. https://doi.org/10.1016/S0032-3861(98)00448-0 (1999).
44. Vynck, V. D. & Goethals, E. J. Synthesis and polymerization of N,N-diallylpyrrolidinium bromide. *J. Macromol. Rapid Commun.* **18**, 149–156. https://doi.org/10.1002/marc.1997.030180212 (1997).
45. Bezdomnikov, A. A. et al. Study of Lithium-Extraction systems based on Benzo-15-Crown-5 ether and Alkylimidazolium-Based ionic liquid. *Molecules* **28**, 935. https://doi.org/10.3390/molecules28030935 (2023).

46. Alexandratos, S. D. & Ion-Exchange Resins A retrospective from industrial and engineering chemistry research. *Ind. Eng. Chem. Res.* **48**, 388–398. https://doi.org/10.1021/ie801242v (2009).
47. Kunin, R., Meitzner, E. A., Oline, J. A., Fisher, S. A. & Frisch, N. Characterization of Amberlyst 15. Macroreticular sulfonic acid cation exchange resin. *I&EC Prod. Res. Dev.* **1**, 140–144. https://doi.org/10.1021/i360002a016 (1962).
48. Al Alshuiael, S. M. & Al-Ghouti, M. A. Development of a novel tailored ion-imprinted polymer for recovery of lithium and strontium from reverse osmosis concentrated Brine. *Sep. Purif. Technol.* **295**, 121320. https://doi.org/10.1016/j.seppur.2022.121320 (2022).
49. Hong, H. et al. Granulation of li+1.33Mn1.67O4 (LMO) through the use of cross-linked Chitosan for the effective recovery of li++ from seawater. *Chem. Eng. J.* **234**, 16–22. https://doi.org/10.1016/j.cej.2013.08.060 (2013).
50. Huang, W., Liu, S., Liu, J., Zhang, W. & Pan, J. 2-Methylol-12-crown-4 ether immobilized polyhipes toward recovery of lithium(I). *New. J. Chem.* **42**, 16814–16822. https://doi.org/10.1039/C8NJ01961D (2018).
51. Bai, X., Dai, J., Ma, Y., Bian, W. & Pan, J. 2-(Allyloxy) methylol-12-crown-4 ether functionalized polymer brushes from porous polyhipe using UV-initiated surface polymerization for recognition and recovery of lithium. *Chem. Eng. J.* **380**, 122386. https://doi.org/10.1016/j.cej.2019.122386 (2020).
52. Ali, S. A. & Mazumder, M. A. J. A new resin embedded with chelating motifs of biogenic methionine for the removal of Hg(II) at Ppb levels. *J. Hazard. Mater.* **350**, 169–179. https://doi.org/10.1016/J.JHAZMAT.2018.02.033 (2018).
53. Haghseresht, F. & Lu, G. Q. Adsorption characteristics of phenolic compounds onto coal-reject-derived adsorbents. *Energy Fuels.* **12**, 1100–1107. https://doi.org/10.1021/ef9801165 (1998).
54. Kumar, K. V. et al. Characterization of the adsorption site energies and heterogeneous surfaces of porous materials. *J. Mater. Chem. A.* **7**, 10104–10137. https://doi.org/10.1039/c9ta00287a (2019).
55. Nandiyanto, A. B. D. et al. Isotherm adsorption characteristics of carbon microparticles prepared from pineapple Peel waste. *Commun. Sci. Technol.* **5**, 31–39. https://doi.org/10.21924/cst.5.1.2020.176 (2020).
56. Temkin, J. M. & Pyzhev, V. Kinetics of ammonia synthesis on promoted iron catalysts. *Acta Physicochim URSS.* **12**, 217–222 (1940). https://ci.nii.ac.jp/naid/20000744365/
57. Liu, H., Cai, X., Wang, Y. & Chen, J. Adsorption mechanism-based screening of cyclodextrin polymers for adsorption and separation of pesticides from water. *Water Res.* **45**, 3499–3511. https://doi.org/10.1016/J.WATRES.2011.04.004 (2011).
58. Boda, A., Ali, S. M., Rao, H. & Ghosh, S. K. Ab initio and density functional theoretical design and screening of model crown ether based ligand (host) for extraction of lithium metal ion (guest): effect of donor and electronic induction. *J. Mol. Model.* **18**, 3507–3522. https://doi.org/10.1007/s00894-011-1348-1 (2012).
59. De, S., Ali, S. M., Shenoi, M., Ghosh, S. K. & Maity, D. K. Conformational effect on the Preferential binding of alkali metal cation with crown ether: a molecular level investigation, desalin. *Water Treat.* **12**, 93–99. https://doi.org/10.5004/dwt.2009.947 (2009).

Acknowledgements

The facilities provided by KFUPM are gratefully acknowledged. The authors would also like to acknowledge the financial support through the Distinguished University Professor Award (# DUP23102) and the internal project (# INMW2109) provided by KFUPM.

Author contributions

Khaled M. Ossoss: Methodology, Formal Analysis, Experimental, Writing original draft, Shaikh A. Ali: Conceptualization, Writing – review & editing, Supervision, Mohammad N. Siddiqui: Conceptualization, Writing – review & editing.

Declarations

Competing interests

The authors declare no competing interests.

Additional information

Correspondence and requests for materials should be addressed to S.A.A.

Reprints and permissions information is available at www.nature.com/reprints.

Publisher's note Springer Nature remains neutral with regard to jurisdictional claims in published maps and institutional affiliations.